Available online at www.sciencedirect.com

ScienceDirect

Cognitive Systems Research xxx (2018) xxx–xxx

Cognitive Systems RESEARCH

www.elsevier.com/locate/cogsys

Medical image denoising by using discrete wavelet transform: Neutrosophic theory new direction

T.E. Aravindan [a,*], R. Seshasayanan [b], K.S. Vishvaksenan [c]

[a] *Sathyabama University, Chennai, India*
[b] *Dept of ECE, Anna University, Chennai, India*
[c] *SSN College of Engineering, Chennai, India*

Received 19 August 2018; received in revised form 23 October 2018; accepted 26 October 2018

Abstract

Medical images are corrupted by noises during the transmission and reception process. Hence noise reduction has been a conventional issue in medical image processing. The main aim of this work is to denoise the high noise density image efficiently, with minimal computation cost. In this paper, an image denoising technique based on Discrete Wavelet Transform (DWT) and Social Spider Optimization (SSO) algorithm is proposed. In Gaussian noise, salt & pepper and speckle noise are added, in which DWT is applied. The wavelet coefficient optimization process is performed for optimizing the coefficient value with the help of SSO. Then in this wavelet-optimized parameter, the inverse DWT (IDWT) is applied. The proposed technique reduces the noise from image more adequately. Performance results using MATLAB, demonstrate that SSO performs better than the other traditional techniques by minimizing the mean square error (MSE).

Keywords: Medical images; Discrete Wavelet Transform (DWT); Social Spider Optimization Algorithm (SSO); Peak Signal to Noise Ratio (PSNR)

1. Introduction

Denoising is a procedure of removing noise from a signal. All recording devices such as analog and digital have attributes which are susceptible to noise. Noise is included to an image during catching or transmission of the image (Kaur, 2014; Khan, Jain, & Khare, 2012). Medical images are regularly affected by noises due to machine specifications, detector specifications and surroundings (Somnath & Mukhopadhyay, 2013). The fundamental objective of image denoising is to suppress noise from images while protecting their features, namely meaningful edges or texture details (Yang, Wang, Niu, & Liu, 2014). Image denoising intends to recover the unknown original image from a noisy estimation or polluted perception and upgrade the contrast (Kaizhi, Zhang, & Ding, 2014). Being the most straightforward possible inverse problem, it gives an advantageous platform over which image processing thoughts and procedures can be surveyed (Wang, Yang, Zhang, & Fu, 2013). Generally, most continuous distortions are due to the corruption by additive noise (Gaussian), salt & pepper noise and multiplicative noise (speckle) with various attributes (Bhandar, Kumar, Kumar, & Singh, 2016). Additionally, the energy of the noise is distributed among each coefficients of the wavelet domain.

1.1. Neutrosophics set (NS) theory

Neutrosophics originate their places into modern research; we have established the notions of neutrosophic crisp sets, neutrosophic crisp point and neutrosophic topology on crisp sets (Salama, ElGhawalby, & Ali, 2017). Neutrosophy is a branch of philosophy, initiated by

* Corresponding author.
E-mail address: aravindante2018@gmail.com (T.E. Aravindan).

https://doi.org/10.1016/j.cogsys.2018.10.027
1389-0417/

Nomenclature

$d_{i,j}$	Euclidian distance	P_{SEri}	probability
MSE	Mean Square Error	ra	radius of mating
NSE	entire population	SSO	Social Spider Optimization
NSE_f	number of female spider	SE_{rnew}	new spider candidate
NSE_m	number of male spiders	SE_{rwo}	worst spider
po_j^{high}	upper initial parameter bound	Vib	vibration
po_j^{low}	lower initial parameter bound	w_i	weight
$PSNR$	Peak Signal to Noise Ratio		

Smarandache in 1980, which studies the origin, nature and scope of neutralities, as excellent as their relations with distinctive ideational spectra (Sahin & Kargın, 2018). In neutrosophic sets, we have truth membership, indeterminacy membership and falsity membership functions, which are independent (Islam & Ray, 2018). Contrasted to additional uncertainty theories, the neutrosophic set can compact with indeterminacy situation (Alias, Mohamad, & Shuib, 2018). It has been the base for increasing of new techniques to handle indeterminate and incompatible information as neutrosophic sets an neutrosophic logic and particularly in decision making problems (Alava, Figueroa, Alcivar, & Vazquez, 2018). Neutrosophic means based on three components T (truth-membership), I (indeterminacy), and F (falsehood non-membership) (Smarandache, 2016). Neutrosophic sets are characterized by three independent degrees (Mohamed, Abdel-Basset, Zaied, & Smarandache, 2017). Each of three independent components of NS belongs to $[^{-}0, 1^{+}]$ (Dalapati & Pramanik, 2018). It is a simplification of Fuzzy set theory and intuitionistic Fuzzy set theory. This theory is considered as entire representation of a mathematical model of an actual world problem (Chalapathi & Kiran Kumar, 2017).

1.2. Problem statement and proposed solution

The wavelet transform of the original and noise signal are combined together to yield wavelet transform of a noisy signal. Hence the noise power can be compressed to a greater extent with the main signal features remain unchanged (Nasri & Nezamabadi-pour, 2009). While the wavelet transform provides the frequency illustration of raw signal at any time instant, the Fourier transform provides the frequency-amplitude illustration of the raw signal (Singh & Wadhwani, 2015a). Because of the nearness of noise, even the specialists with adequate experience will most likely be unable to draw accurate and valuable data from the images (Bhadauria & Dewal, 2013). The DWT which is generally utilized for time-frequency localization, multi-resolution examination, edge detection and decorrelation, has been successfully used in the MR image denoising (Kai, Cheng, Li, & Gao, 2018). The DWT based denoising, named as wavelet shrinkage, works by thresholding (often, nonlinearly) the wavelet coefficients before recreating the denoised signal from wavelet decomposition coefficients (Rajpoot, Rajpoot, & Noble, 2008). Initially, the optimum wavelet basis and decomposition layer are selected through simulation (Chen, Cheng, & Liu, 2017). In this paper, wavelet thresholding strategies are connected to an image. It removes noise by removing coefficients that are unimportant with respect to some threshold. The decision of this threshold decides the adequacy of denoising (Al Jumah, 2013). Finally, the performances are evaluated in terms of the metrics MSE and PSNR (Soni & Roy, 2014).

The upcoming sections described as Section 2 literature review of the work, Section 3 expressed the proposed methodology in detail, Section 4 explained the results and discussion finally concluded the work in Section 5.

2. Literature review

Year/author/ reference	Techniques	Remarks
In 2018, Jianjun Yuan (Yuan, 2018)	Alternating Direction Method of Multipliers (ADMM)	Investigational outcomes reveal that the proposed technique was proficient, and has superior denoising capability than the state-of-the-art models.
In 2017, Sushil Kumar (Kumar, 2017)	Discrete Wavelet Transform (DWT)	The PSNR for the SLT based Block Shrink was better alternative as it gives better time confinement and better signal compression contrasted with the established DWT.

Please cite this article in press as: Aravindan, T. E., et al. Medical image denoising by using discrete wavelet transform: Neutrosophic theory new direction. *Cognitive Systems Research* (2018), https://doi.org/10.1016/j.cogsys.2018.10.027

In 2017, Ruxin Zhao et al. (Zhao, Luo, & Zhou, 2017)	Elite Opposition-based SSO algorithm (EOSSO)	The outcomes of results demonstrate that EOSSO could get a precise arrangement and converges in short iterations with high security.
In 2015, Sonali Singh and Sulochana Wadhwani (Singh & Wadhwani, 2015b)	Wavelet transform	Outcomes got utilizing that strategy based on genetic algorithm beats in contrast with different strategies namely Visu shrink, Sure shrink and Bayes shrink. It gives better outcomes as far as visual quality and PSNR.
In 2015, Nadir Mustafa et al. (Mustafa, Li, Khan, & Gless, 2015)	Discrete Wavelet Transform (DWT)	Experimental work has been conducted by utilizing the parameters namely PSNR & MSE from numerical outcomes for productive de-noising of noisy medical image.
In 2011, Sachin D Ruikar and Dharmpal D Doye (Ruikar & Doye, 2011)	Wavelet transform	In this work, existing method was extended to yield a thorough assessment of the proposed strategy. Outcomes based on various noises were performed.

3. Proposed methodology

In this paper, an image denoising technique based on DWT and SSO algorithm is proposed. The medical images are considered as input by applying the noises such as Gaussian noise, salt and pepper noise and speckle noise. After applying these noises, DWT has been applied for medical images to disintegrate the original image into components and coefficients. The Haar wavelet is used to separate the bands and threshold operation is carried out in three bands. The wavelet coefficient optimization process is performed for optimizing the coefficient value with the help of SSO algorithm. Finally, by applying the IDWT on thresholded coefficients, the denoised image is obtained and then the PSNR evaluation is utilized for finding the superior performance shown in Fig. 1.

The actual image is in spatial domain it is hard to compute that's why we convert it into transformation domain.

3.1. Types of various noises

3.1.1. Gaussian noise

Gaussian noise is a type of additive amplifier noise which is independent at each pixel with unique signal intensity. Amplifier noise is the main component of 'red noise' which is having constant noise level in dark portions of images.

3.1.2. Salt-and-pepper noise

Impulsive noise is also called as salt-and-pepper noise or spike noise. This kind of noise is usually present in images. An image with salt-and-pepper noise will contain dark pixels in bright portions and bright pixels in dark portions. This noise is formed by dead pixels, errors due to analog-to-digital conversions, bit errors etc. It can be discarded by applying dark frame subtraction and performing interpolation around dark/bright pixels.

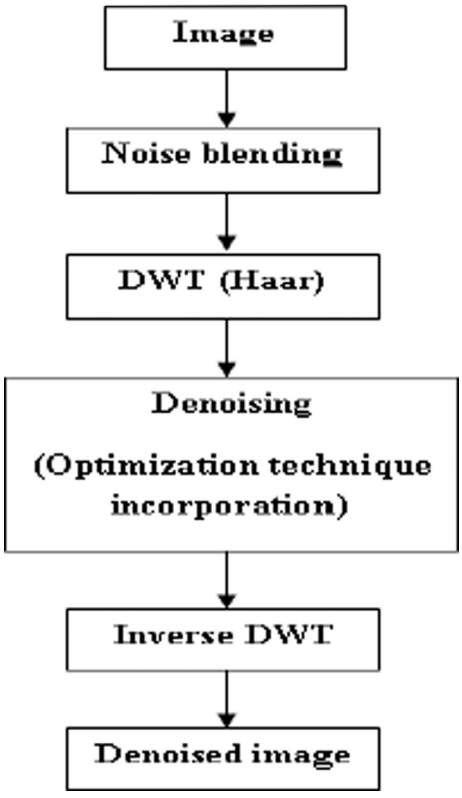

Fig. 1. Flowchart for proposed technique.

Please cite this article in press as: Aravindan, T. E., et al. Medical image denoising by using discrete wavelet transform: Neutrosophic theory new direction. *Cognitive Systems Research* (2018), https://doi.org/10.1016/j.cogsys.2018.10.027

3.1.3. Speckle noise

Speckle noise is a type of granular noise which reduces the quality of active radar and synthetic aperture radar (SAR) images. It is caused by the frequent fluctuations in the return signal of an object. Image interpolation in images with Speckle noise becomes more difficult. In oceanography speckle noise is caused by signals from elementary scatters, the gravity-capillary ripples and manifests as a pedestal image.

3.2. Discrete Wavelet Transform (DWT)

In numerical and functional investigations, DWT is any wavelet transform in which the wavelets are discretely inspected. The Hungarian mathematician Alfréd Haar invented the first DWT. The mathematical manipulation, which implies analysis and synthesis, is called discrete wavelet transform and inverse discrete wavelet transform. An image can be decomposed into a sequence of different spatial resolution images using DWT. It decomposes the data into four different bands LL, HL, LH, and HH. The sub-band LL is a reduced resolution corresponding to the low frequency part of the image. The other three sub-bands HL, LH and HH are the high frequency parts in the vertical, horizontal, and diagonal directions, respectively. The Haar transformation technique is the simplest among all the wavelet transformation techniques which meet our requirements. In this technique, low-pass filtering is done by finding the average of two adjacent pixel values and high-pass filtering is done by finding the difference between the two adjacent pixel values.

3.3. Threshold operation

In threshold operation, three different (horizontal, vertical, and diagonal) sub-bands are taken. From these three subbands, the optimum coefficient parameter is determined using the SSO algorithm which is explained in the next section in detail.

$$S(x) = Sign\ (x)\ (|x|\ -\ t)\ *\ (|x| > t) \tag{1}$$

where t is a threshold.

3.4. Social Spider Optimization (SSO)

SSO is a swarm optimization algorithm from the social-spider colony. In SSO, the searching space is a collective web where all the social spiders are dependent on the other. There are two unique spiders: males and females. Every spider is directed by a set of different evolutionary operators, which emulate distinctive collective behaviors that are generally estimated inside the colony, depending on genders.

Initially, the female and male spiders are characterized in the searching space. The number of females NSE_f is randomly selected inside the scope of 65–90% of the entire population NSE. Thusly, NSE_f is ascertained by the following condition:

$$NSE_f = floor\ \ [(\,0.9 - rand.025\,)\,.\ NSE] \tag{2}$$

where rand represents random number in the range of [0, 1]. The number of male spiders NSE_m is calculated as the complement between NSE and NSE_f as

$$NSE_m = NSE - NSE_f \tag{3}$$

Hence the full population SE_r with NSE members is categorized into the groups F and M.

3.4.1. Initialization

The whole population is randomly initialized. The set SE_r of NSE spider positions are initialized. These values are randomly and consistently conveyed between the pre-indicated lower bound po_j^{low} and the upper bound po_j^{high}, represented by the following expressions:

$$f_{i,j}^0 = po_j^{low} + rand(0,1).(po_j^{high} - po_j^{low}) \quad (i = 1,2...NSE_f, j = 1,2,..n) \tag{4}$$

$$m_{k,j}^0 = po_j^{low} + rand(0,1).(po_j^{high} - po_j^{low}) \quad (k = 1,2...NSE_m, j = 1,2,..n) \tag{5}$$

where j, i and k are individual indexes and zero represents the initial population. Hence, $f_{i,j}$ is the j^{th} parameter of the i^{th} female spider position.

Then the radius of mating is computed by

$$ra = \frac{\sum_{j=1}^{n}(po_j^{high} - po_j^{low})}{2.n} \tag{6}$$

The randomly generated initial solution is coefficient values and the number of spiders are 4, the range for the solution is (−1 to 1).

3.4.2. Fitness function

In this algorithm, each spider gets a weight w_i which speaks to the solution quality which is related to the spider i of population SE.

For finding coefficient value optimization, the fitness function in terms of Peak Signal to Noise Ratio (PSNR) is shown as below:

$$Fitness\ =\ Avg\ (PSNR) \tag{7}$$

$$= Avg\left[20\log_{10}\left(\frac{255^2}{MSE}\right)dB\right]$$

where MSE denotes the Mean Square Error between the original and denoised image given by

$$MSE\ =\ \frac{1}{MN}\sum_{i=1}^{M}\sum_{j=1}^{N}\left(U_{ij} - V_{ij}\right)^2 \tag{8}$$

where M, N are width and height of image V–Noisy image U–original image.

The weight of the spider is determined as

$$w_i = \frac{J(SE_{ri}) - worst_{SE_r}}{best_{SE_r} - worst_{SE_r}} \tag{9}$$

where $J(SE_{ri})$ is the value of fitness function determined by the position of spider SE_i with respect to the objective func-

Please cite this article in press as: Aravindan, T. E., et al. Medical image denoising by using discrete wavelet transform: Neutrosophic theory new direction. *Cognitive Systems Research* (2018), https://doi.org/10.1016/j.cogsys.2018.10.027

tion J(.) The values $worst_{sEr}$ and $best_{sEr}$ are defined as below:

$$best_{sEr} = \min_{k\in\{1,2,\ldots N\}}(J(SE_r)) \text{ and } worst_{sEr} = \max_{k\in\{1,2,\ldots N\}}(J(SE_r)) \quad (10)$$

3.4.3. Determining vibrations of spiders

The vibrations are based on the weight and separation of the spiders. With a specific end goal to emulate this method, the vibrations observed by the member i due to data transmission by the member j is given below:

$$Vib_{i,j} = w_j.e^{-d_{ii,j}^2} \quad (11)$$

where the $d_{i,j}$ is the distance between the spiders i and j, $d_{i,j} = \|S_{ri} - S_{rj}\|$.

3.4.3.1. Cooperative operators. In this cooperative operator method, two types of operators are explained beneath namely female and male cooperative operators.

3.4.3.2. Female cooperative operator. In order to imitate the cooperative activities of the female i, a new operator is characterized by considering the change of position of i (CP_i) at each iteration. CP_i is derived as a mix of three distinct components. The first contains the change concerning the closest part to i that contains a larger weight and creates the vibration $Vibx_i$. The second one considers the change with respect to the best member of SE_r who delivers the vibration $Viby_i$. The third one joins an irregular improvement.

$$Vibx_i = w_x.e^{-d_{i,y}^2}, \; Viby_i = w_y.e^{-d_{i,x}^2} \quad (12)$$

A uniform random number r_m is created in the range [0, 1]. If r_m is <PF, an attraction movement is created; Otherwise, a repulsion movement is created. Hence, such operator can be represented as below:

$$f_i^{k+1} = \begin{cases} f_i^k + \alpha.Vibx_i.(SE_{ry} - f_i^k) + \beta.Viby_i.(SE_{rx} - f_i^k) \\ \quad +\delta.(rand - 12) \; with \quad probability \; PF \\ f_i^k - \alpha.Vibx_i.(SE_{ry} - f_i^k) - \beta.Viby_i.(SE_{rx} - f_i^k) \\ \quad +\delta.(rand - 12) \; with \quad probability \; 1 - PF \end{cases} \quad (13)$$

wherever α, β, δ and *rand* are random numbers in the range of [0, 1] and k denotes the iteration index. The individuals SE_{rx} and SE_{ry} symbolize the nearest member to i that has a larger weight and the best member of SE_r, respectively.

3.4.3.3. Male cooperative operator. Male individuals, with a weight value over the median value inside the male population, are viewed as the overwhelming people D. Those below the middle esteem are marked as non-prevailing ND males. To actualize such calculation, the male population M ($M = \{m_1, m_2, \ldots m_{NSEm}\}$ is masterminded by their weight an incentive in diminishing request. The vibration $Vibw_i$ observed by that individual $i(D_i)$ because of the data passed on by the part $w(D_z)$ with w persistently the nearest female unmistakable to i.

$$Vibw_i = w_z.e^{-d_{i,z}^2} \quad (14)$$

Since records of M concerning the SE_r are expanded by the number of females NSE_f, the median weight is indexed by NSE_{f+m}. Then, position change for the male spider can be derived as:

$$m_i^{k+1} = \begin{cases} m_i^k + \alpha.Vibw_i.(SE_{rf} - m_i^k) + \delta.(rand - 12) if \;\; w_{NSE_{f+i}} > w_{NSE_{f+m}} \\ m_i^k + \alpha.\left(\frac{\sum_{h=1}^{NSEm} m_h^k.w_{NSE_{f+h}}}{\sum_{h=1}^{NSEm} w_{NSE_{f+h}}} - m_i^k\right) if \;\; w_{NES_{f+i}} \leqslant w_{NSE_{f+m}} \end{cases} \quad (15)$$

where S_{rf} indicates the nearest female member to the male member i while ($\Sigma_{h-1}^{NSEm} \; m_h^k.W_{NSEf+h}/\Sigma_{h-1}^{NSEm} \; W_{NSEf+h}$) communicate to the weighted mean of M.

By utilizing this operator, two distinct behaviors are delivered. First, the set D is pulled into others keeping in mind the end goal to incite mating. Such conduct permits fusing differing qualities into the population. Second, the set ND is pulled into the weighted mean of M. This reality is utilized to control the pursuit procedure as per the average performance of a subgroup of the population.

3.4.4. Mating process

In mating, the weight of each spider (elements of Tg) characterizes the probability of impact for every person into the new brood. The spiders having a larger weight will probably affect the new item, while components with smaller weight have a lower probability. The impact probability P_{SEri} of every part is allotted by the roulette approach, which is characterized as takes after:

$$p_{SE_{ri}} = \frac{w_i}{\sum_{j\in T^k} w_j} \quad where \; i \in T^g \quad (16)$$

Once the new spider is shaped, it is contrasted with the new spider candidate SE_{rnew} holding the worst spider SE_{rwo} of the colony, as indicated by their weight values (where $w_{wo} = min_{l\epsilon\{1,2,\cdots,NSE\}} \; (w_l)$). On the off chance that the new spider is superior to the worst spider, the new one replaces the worst spider. Something else, the new spider is disposed of and the population does not endure changes. If there should arise an occurrence of substitution, the new spider accepts the gender and index from the supplanted spider. Such certainty guarantees that the entire population S_r keeps up the first rate amongst female and male individuals.

4. Results and discussion

In this result section, MATLAB is used to implement the proposed denoising algorithm. A usual way to denoise is to find a processed image such that it minimizes MSE and increases the value of the PSNR. For study purpose, 10 images have been taken considering various noises. A neutrosophic set (NS) image IM is represented by three element as IM(t,i,f), where t varies in T, i varies in I and

Table 1
PSNR value for different noise level.

Original image	PSNR								
	Gaussian noise level			Salt and pepper noise level			Speckle noise level		
	0.01	0.02	0.03	0.01	0.02	0.03	0.01	0.02	0.03
1	61.71	62.41	63.29	66.77	66.53	66.32	65.12	63.06	62.08
2	61.66	62.53	63.30	66.84	66.62	66.35	65.13	63.06	62.05
3	61.35	62.14	62.95	66.19	65.97	65.76	64.74	62.99	62.07
4	61.21	61.93	62.79	65.83	65.61	65.44	64.56	62.91	62.07
5	61.27	62.02	62.82	65.54	65.34	65.17	64.35	62.72	61.94
6	61.39	62.15	62.89	65.73	65.52	65.34	64.38	62.66	61.86
7	61.35	62.14	62.88	65.75	65.55	65.37	64.46	62.77	61.97
8	61.38	62.21	63.02	65.74	65.56	65.37	64.28	62.53	61.67
9	61.85	62.59	63.40	66.29	66.08	65.88	64.59	62.64	61.70
10	62.10	62.90	63.66	66.72	66.49	66.26	64.81	62.62	61.55

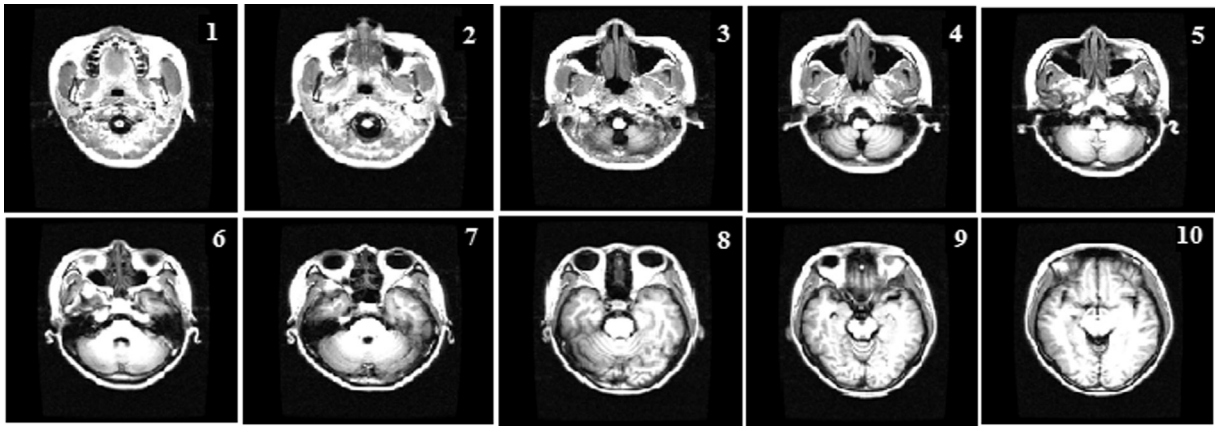

Fig. 2. Original images.

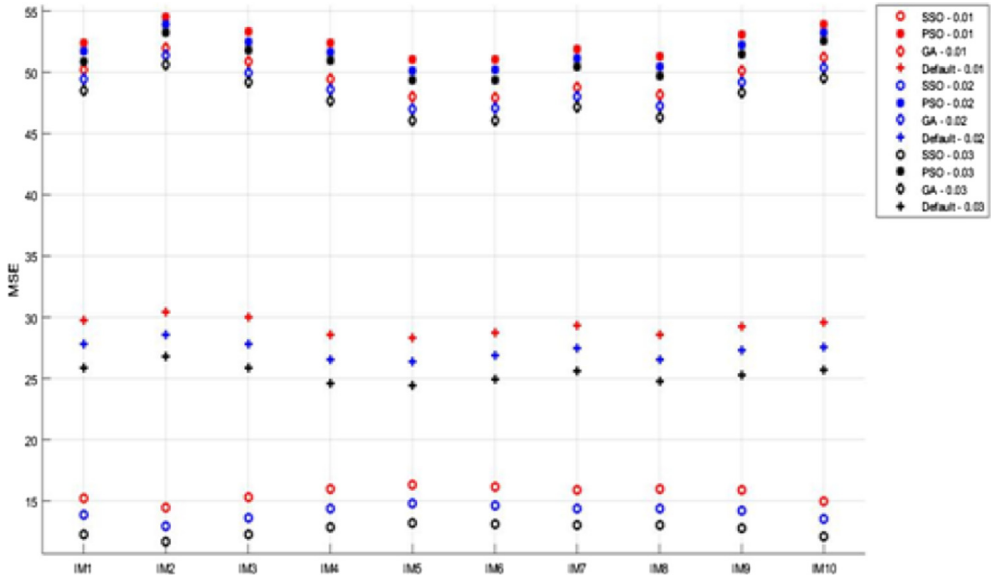

Fig. 3. MSE graph for various Gaussian noise levels for different algorithms.

Please cite this article in press as: Aravindan, T. E., et al. Medical image denoising by using discrete wavelet transform: Neutrosophic theory new direction. *Cognitive Systems Research* (2018), https://doi.org/10.1016/j.cogsys.2018.10.027

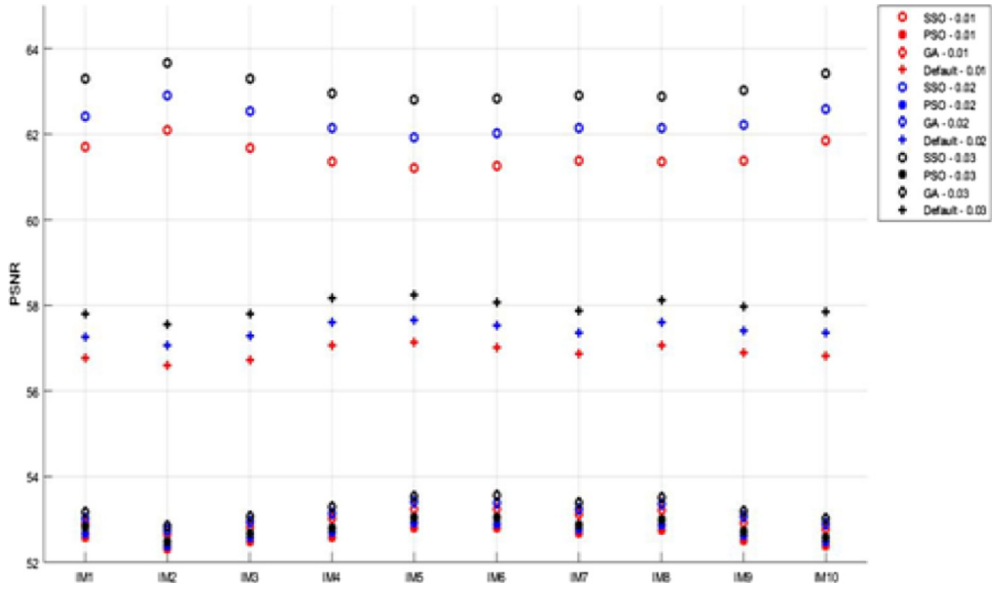

Fig. 4. PSNR graph for various Gaussian noise levels for different algorithms.

f varies in F in the set A of the universal set U. Our picture fuzzy set turns out a particular case of neutrosophic set. Hence, from now on, we too regard picture fuzzy set as standard neutrosophic set (Bui, Phong, & Smarandache, 2016).

Then DWT and threshold operation using SSO algorithm are performed. The performance of the algorithm is evaluated with the brain images from the test database – Osirix. The algorithm was tested at different Gaussian noise levels, Salt and pepper noise levels and Speckle noise levels. Objective Analysis is of two kinds Statistical and Human Visual System, in Statistical analysis Peak Signal to Noise Ratio (PSNR) and Mean Square Error (MSE) performed. In Human Visual System, the Structural Similarity Index Model (SSIM) and Universal Image Quality Index (UIQI) performed. After observing results, the PSNR for Gaussian noise, Salt & pepper noise and Speckle noise is better.

In Table 1, the PSNR value for different noise level has been shown clearly. Gaussian noise level, Salt and pepper noise level and speckle noise level has analyzed and find the PSNR values for 10 images.

Table 1 demonstrates the PSNR value for different noise level and Fig. 2 shows the original images.

In Fig. 3 the MSE graph shown for different Gaussian noise level and different algorithm. The graph exposed

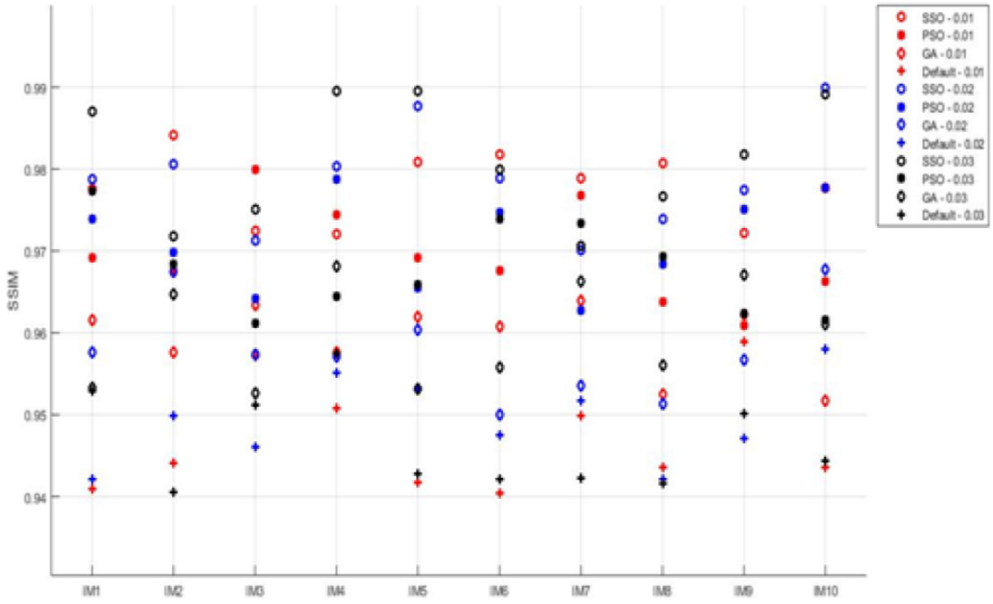

Fig. 5. SSIM graph for various Gaussian noise levels for different algorithms.

Please cite this article in press as: Aravindan, T. E., et al. Medical image denoising by using discrete wavelet transform: Neutrosophic theory new direction. *Cognitive Systems Research* (2018), https://doi.org/10.1016/j.cogsys.2018.10.027

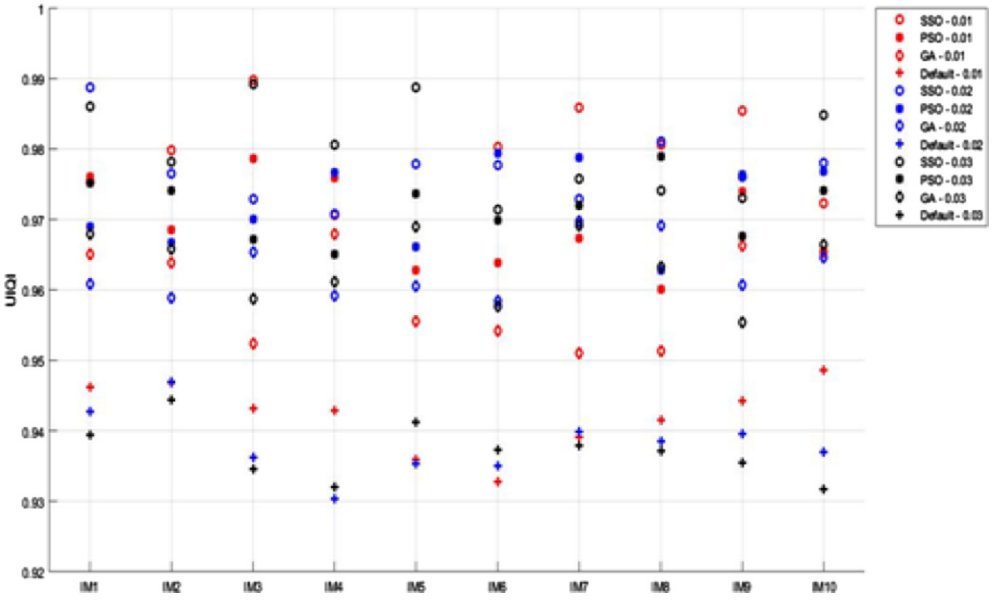

Fig. 6. UIQI graph for various Gaussian noise levels for different algorithms.

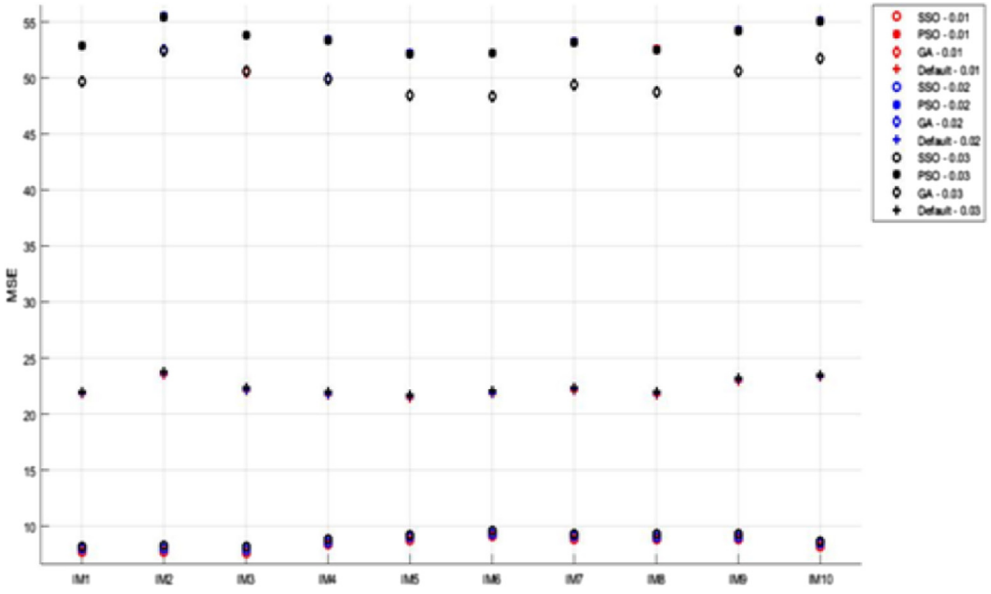

Fig. 7. MSE graph for various Salt and pepper noise levels for different algorithms.

for ten-brain images using different Gaussian noise level (0.01, 0.02 and 0.03) and different algorithms such as SSO, PSO, GA and Default. In this, the MSE value is minimized in SSO-0.03 compared with other techniques.

In Fig. 4, the PSNR graph shown for different Gaussian noise level and different algorithm. The graph exposed for ten-brain images using different Gaussian noise level (0.01, 0.02 and 0.03) and different algorithms such as SSO, PSO, GA and Default. In this, the PSNR value is high in SSO-0.03 compared with other techniques.

In Fig. 5, the SSIM graph shown for different Gaussian noise level and different algorithm. The graph exposed for ten-brain images using different Gaussian noise level (0.01, 0.02 and 0.03) and different algorithms such as SSO, PSO, GA and Default. In this, the SSIM value is high in SSO-0.03 compared with other techniques.

In Fig. 6, the UIQI graph shown for different Gaussian noise level and different algorithm. The graph exposed for ten-brain images using different Gaussian noise level (0.01, 0.02 and 0.03) and different algorithms such as SSO, PSO, GA and Default. In this, the UIQI value is high in SSO-0.03 compared with other techniques.

In Fig. 7, the MSE graph is shown for different noise levels, for different algorithms. The graph exposed for

Please cite this article in press as: Aravindan, T. E., et al. Medical image denoising by using discrete wavelet transform: Neutrosophic theory new direction. *Cognitive Systems Research* (2018), https://doi.org/10.1016/j.cogsys.2018.10.027

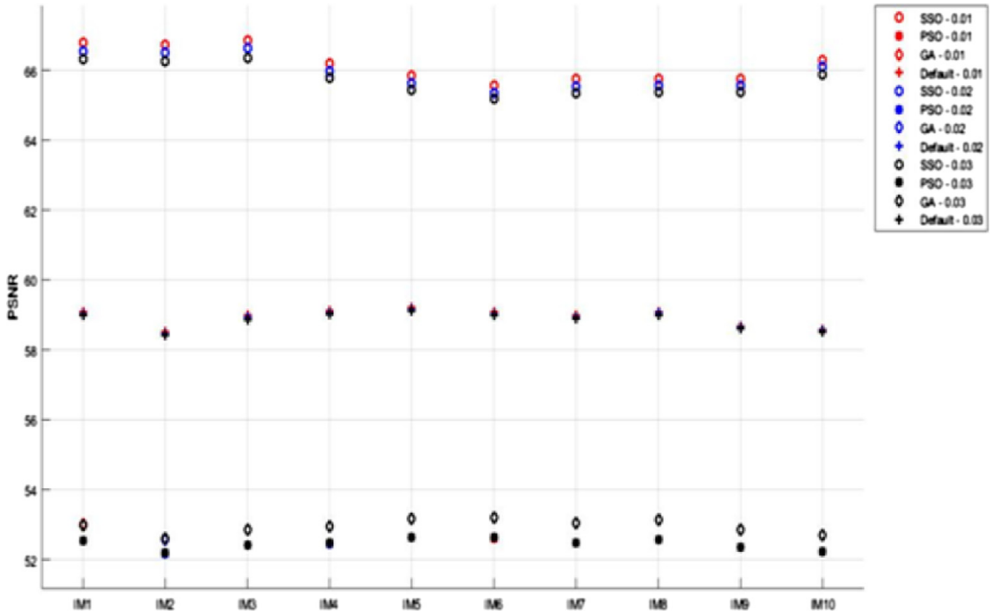

Fig. 8. PSNR graph for various Salt and pepper noise levels for different algorithms.

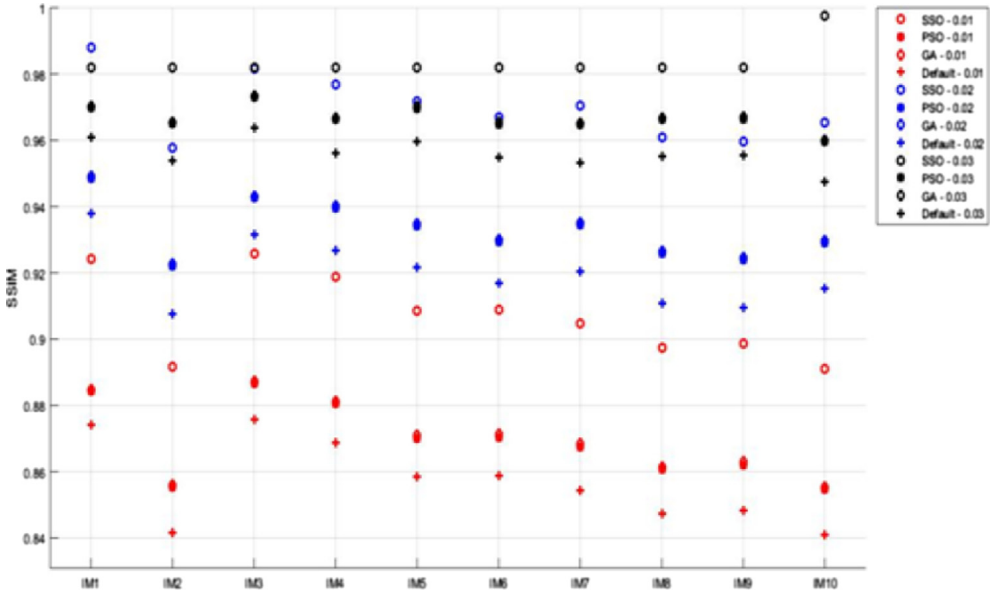

Fig. 9. SSIM graph for various Salt and pepper noise levels for different algorithms.

ten-brain images with noise levels (0.01, 0.02 and 0.03) for different algorithms such as SSO, PSO, GA and Default. In this, the MSE value is minimized in SSO-0.03 compared with other techniques.

In Fig. 8, the PSNR graph is shown for different noise levels, for different algorithms. The graph exposed for ten-brain images with noise levels (0.01, 0.02 and 0.03) for different algorithms such as SSO, PSO, GA and Default. In this, the PSNR value is high in SSO-0.01 compared with other techniques.

In Fig. 9, the SSIM graph is shown for various noise levels for different algorithms. The graph exposed for ten-brain images with noise levels (0.01, 0.02 and 0.03) for different algorithms such as SSO, PSO, GA and Default. In this, the SSIM value is high in SSO-0.03 compared with other techniques.

In Fig. 10, the UIQI graph is presented for various noise levels for different algorithms. The graph exposed for ten-brain images with noise levels (0.01, 0.02 and 0.03) for different algorithms such as SSO, PSO, GA and Default. In this, the UIQI value is high in SSO-0.03 compared with other techniques.

In Fig. 11, the MSE graph demonstrates for different noise levels for different algorithms. The graph exposed

Please cite this article in press as: Aravindan, T. E., et al. Medical image denoising by using discrete wavelet transform: Neutrosophic theory new direction. *Cognitive Systems Research* (2018), https://doi.org/10.1016/j.cogsys.2018.10.027

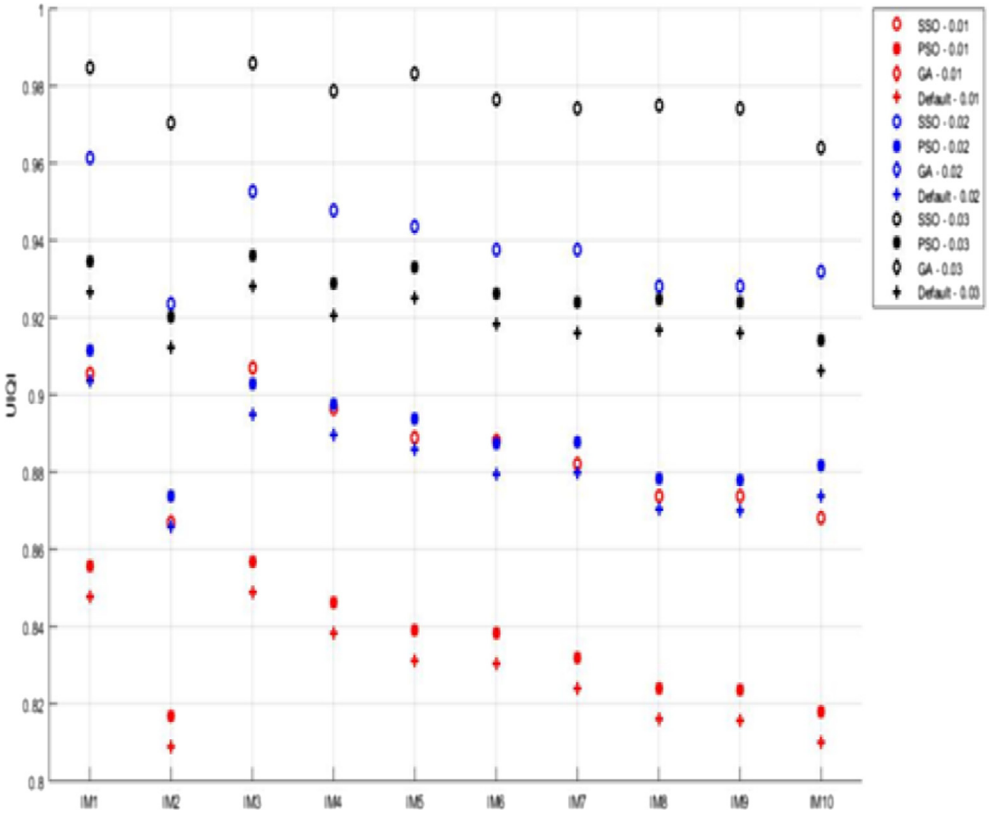

Fig. 10. UIQI graph for various Salt and pepper noise levels for different algorithms.

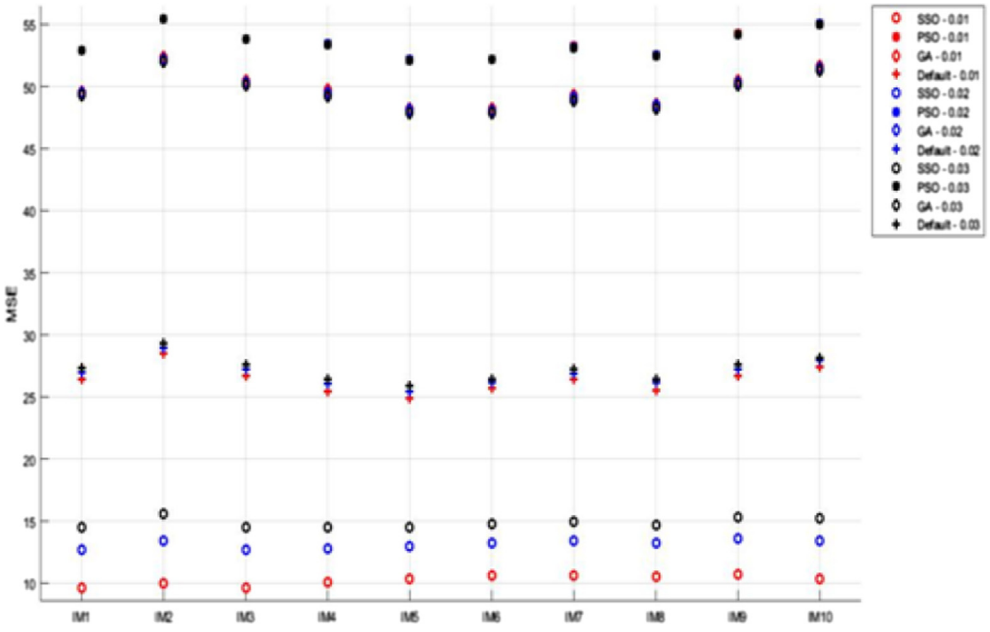

Fig. 11. MSE graph for different Speckle noise levels for different algorithms.

for ten-brain images with noise levels (0.01, 0.02 and 0.03) for different algorithms such as SSO, PSO, GA and Default. In this, the MSE value is minimized in SSO-0.01 compared with other techniques.

In Fig. 12, the PSNR graph demonstrates for different noise levels for different algorithms. The graph exposed for ten-brain images with noise levels (0.01, 0.02 and 0.03) for different algorithms such as SSO, PSO, GA and Default. In this, the PSNR value is high in SSO-0.01 compared with other techniques.

In Fig. 13, the SSIM graph demonstrates for different noise levels for different algorithms. The graph exposed

Please cite this article in press as: Aravindan, T. E., et al. Medical image denoising by using discrete wavelet transform: Neutrosophic theory new direction. *Cognitive Systems Research* (2018), https://doi.org/10.1016/j.cogsys.2018.10.027

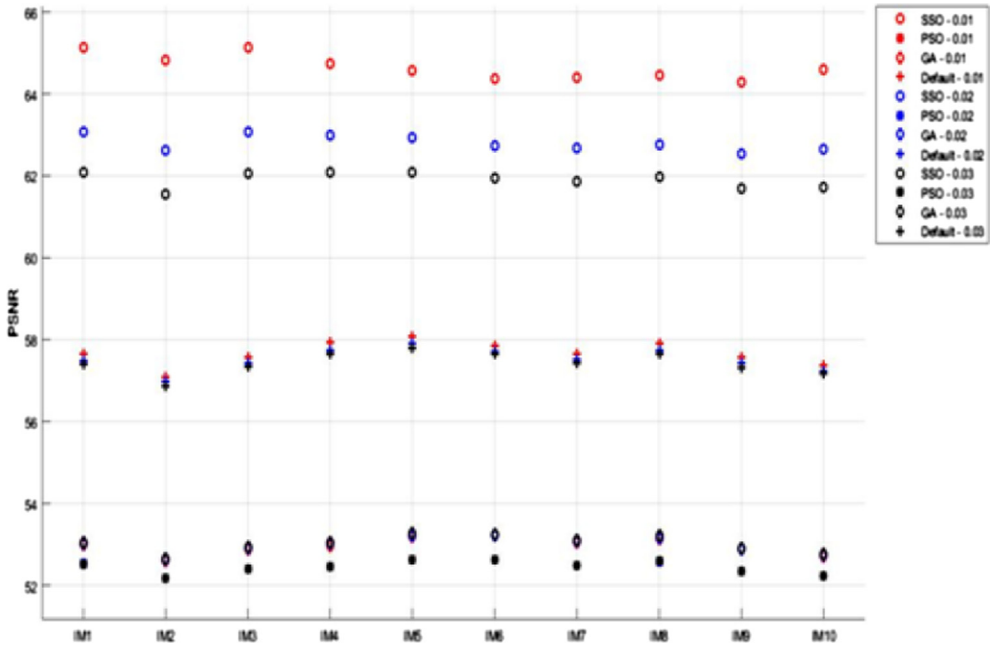

Fig. 12. PSNR graph for different Speckle noise levels for different algorithms.

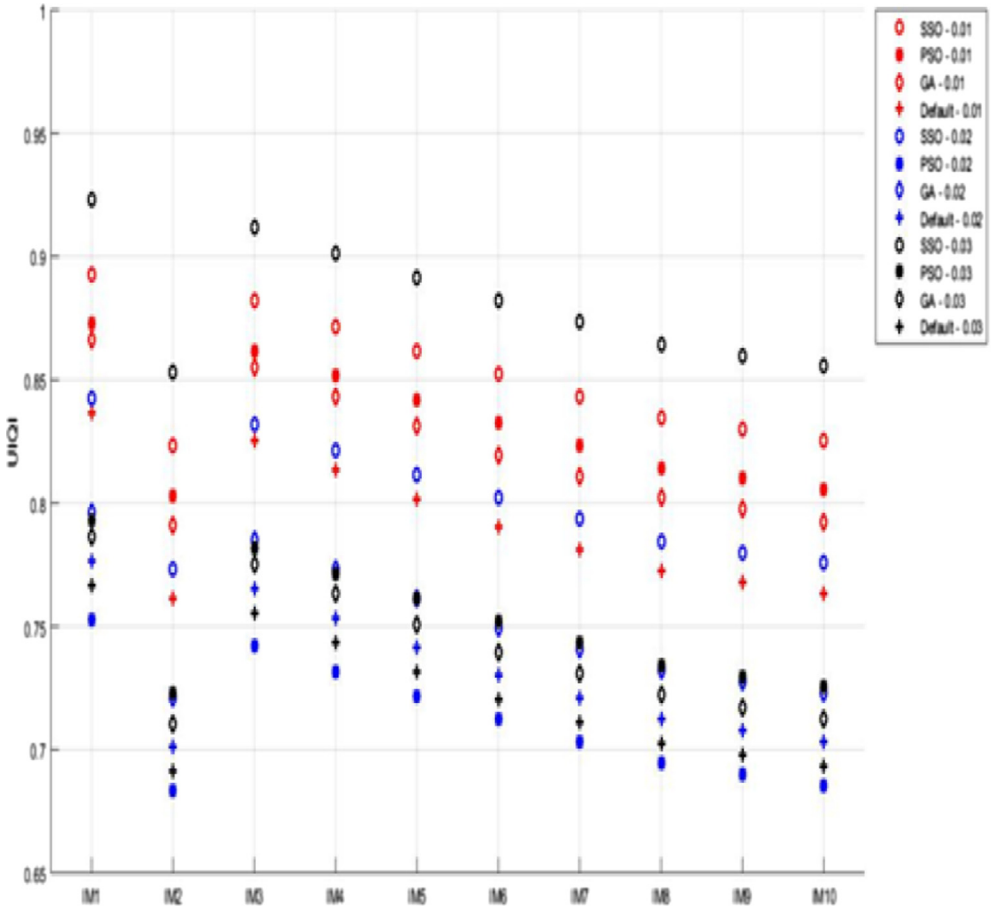

Fig. 13. SSIM graph for various Speckle noise levels for different algorithms.

Please cite this article in press as: Aravindan, T. E., et al. Medical image denoising by using discrete wavelet transform: Neutrosophic theory new direction. *Cognitive Systems Research* (2018), https://doi.org/10.1016/j.cogsys.2018.10.027

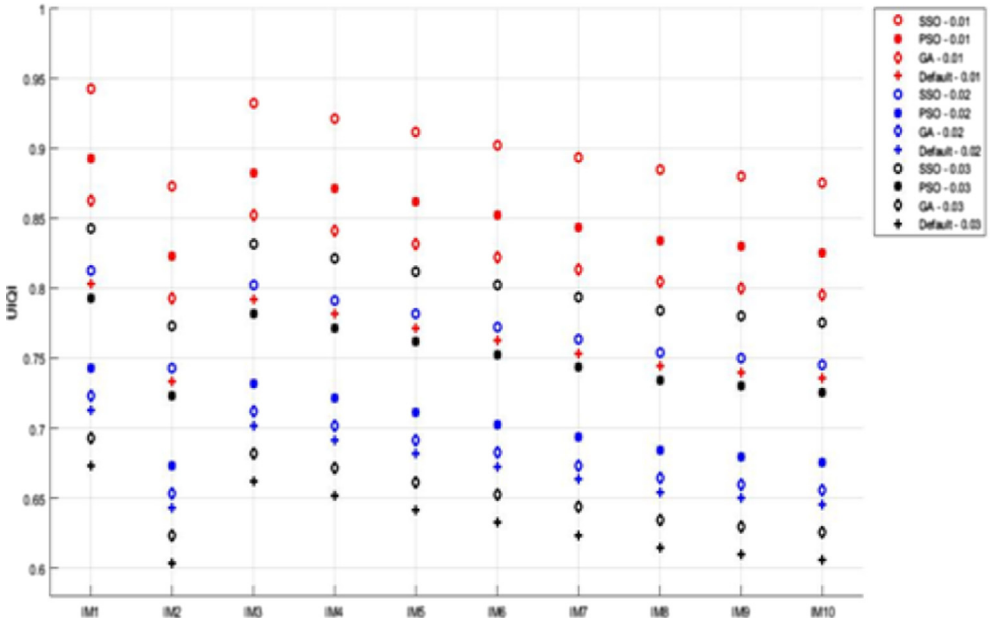

Fig. 14. UIQI graph for different Speckle noise levels for different algorithms.

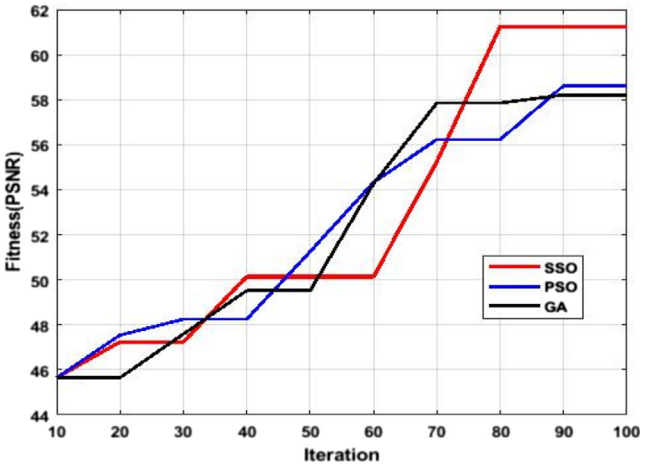

Fig. 15. Convergence graph.

for ten-brain images with noise levels (0.01, 0.02 and 0.03) for different algorithms such as SSO, PSO, GA and Default. In this, the SSIM value is high in SSO-0.03 compared with other techniques.

In Fig. 14, the UIQI graph demonstrates for different noise levels for different algorithm. The graph exposed for ten-brain images with noise levels (0.01, 0.02 and 0.03) for different algorithms such as SSO, PSO, GA and Default. In this, the UIQI value is high in SSO-0.01 compared with other techniques.

From the above Fig. 15, three different algorithms performed namely SSO, PSO and GA from this SSO algorithm is better when compared with other techniques. The time complexity of SSO is 145.56 sec, PSO is 101.67 sec and GA is 78.89 sec. From the graph, SSO algorithm increased from 10th iteration the fitness value is 45.8 then slightly improved up to 100th iteration of fitness 61.8. The PSO algorithm increased 10th iteration the fitness value is 45.8 then slightly improved up to 100th iteration of fitness 58.1. Finally, GA algorithm increased 10th iteration the fitness value is 45.8 then slightly improved up to 100th iteration of fitness 58.

5. Conclusion

This paper proposed a denoising (SSO) algorithm for the brain images, which are corrupted with various types of noises. The execution of the algorithm is tested with the brain images from the test database – Osirix. Objective Analysis is of two sorts Statistical and Human Visual System. In Statistical analysis, PSNR and MSE are measured. In Human Visual System, the SSIM and UIQ are measured. After observing the outcomes, the PSNR for various types of noises found to be better. It also demonstrates that MSE is diminished to a larger level and PSNR is maximized. Experimental outcomes demonstrate that the SSO technique based on the wavelet transform, produces better results as far as PSNR and visual impacts. In future, various techniques and various datasets will be used for more analysis and image quality improvements.

Appendix A. Supplementary material

Supplementary data to this article can be found online at https://doi.org/10.1016/j.cogsys.2018.10.027.

References

Al Jumah, A. (2013). Denoising of an image using discrete stationary wavelet transform and various thresholding techniques. *Journal of Signal and Information Processing, 4*, 33–41.

Alava, M. V., Figueroa, S. P. D., Alcivar, H. M. B., & Vazquez, M. L. (2018). Single valued neutrosophic numbers and analytic hierarchy process for project selection. *Neutrosophic Sets and Systems, 21*, 122–130.

Alias, S., Mohamad, D., & Shuib, A. (2018). Rough, neutrosophic multisets relation with application in marketing strategy. *Neutrosophic Sets and Systems, 21*, 36–55.

Bhadauria, H. S., & Dewal, M. L. (2013). Medical image denoising using adaptive fusion of curvelet transform and total variation. *Computers and Electrical Engineering, 39*, 1451–1460.

Bhandari, A. K., Kumar, D., Kumar, A., & Singh, G. K. (2016). Optimal, sub-band adaptive thresholding based edge preserved satellite image denoising using adaptive differential evolution algorithm. *Neurocomputing, 174*, 698–721.

Chalapathi, T., Kiran, R. V. M. S. S., & Kumar (2017). Neutrosophic graphs of finite groups. *Neutrosophic Sets and Systems, 15*, 22–30.

Chen, Yong, Cheng, Y., & Liu, H. (2017). Application of improved wavelet adaptive threshold de-noising algorithm in FBG demodulation. *Optik – International Journal for Light and Electron Optics, 132*, 243–248.

Cuong, B. C., Phong, P. H., & Smarandache, F. (2016). Standard neutrosophic soft theory: Some first results. *Neutrosophic Sets and Systems, 12*, 80–91.

Dalapati, S., & Pramanik, S. (2018). A revisit to NC-VIKOR based MAGDM strategy in neutrosophic cubic set environment. *Neutrosophic Sets and Systems, 21*, 131–141.

Islam, S., & Ray, P. (2018). Multi-objective, portfolio selection model with diversification by neutrosophicoptimization technique. *Neutrosophic Sets and Systems, 21*, 74–83.

Kai, H., Cheng, Q., Li, B., & Gao, X. (2018). The complex data denoising in MR images based on the directional extension for the undecimated wavelet transform. *Biomedical Signal Processing and Control, 39*, 336–350.

Kaizhi, W., Zhang, X., & Ding, M. (2014). Curvelet based nonlocal means algorithm for image denoising. *International Journal of Electronics and Communications (AEÜ), 68*, 37–43.

Kaur, T. (2014). Image, denoising algorithms and DWT: A review. *International Journal of Computer Science and Information Technologies, 5*(5), 6135–6137.

Khan, S., Jain, A., & Khare, A. (2012). Image denoising based on adaptive wavelet thresholding by using various shrinkage methods under different noise condition. *International Journal of Computer Applications, 59*(20), 13–17.

Kumar, S. (2017). Image de-noising using wavelet-like transform. *International Journal of Advance Research and Innovation, 5*(1), 70–72.

Mohamed, M., Abdel-Basset, M., Zaied, A. N. H., & Smarandache, F. (2017). Neutrosophic integer programming problem. *Neutrosophic Sets and Systems, 15*, 3–7.

Mukhopadhyay, S., & Mandal, J. K. (2013). Wavelet based denoising of medical images using sub-band adaptive thresholding through genetic algorithm. *Procedia Technology, 10*, 680–689.

Mustafa, N., Li, J.-P., Khan, S. A., & Gless, M. (2015). Medical image denoising schemes using wavelet threshold techniques with various noises. In *Proceedings of international computer conference on wavelet active media technology and information processing* (pp. 283–289).

Nasri, M., & Nezamabadi-pour, H. (2009). Image, denoising in the wavelet domain using a new adaptive thresholding function. *Neurocomputing, 72*, 1012–1025.

Rajpoot, K., Rajpoot, N., & Noble, J. A. (2008). Discrete wavelet diffusion for image denoising. In *International conference on image and signal processing* (pp. 1–8).

Ruikar, S. D., & Doye, D. D. (2011). Wavelet based image denoising technique. *International Journal of Advanced Computer Science and Applications, 2*(3), 49–53.

Sahin, M., & Kargın, A. (2018). Neutrosophic triplet normed ring space. *Neutrosophic Sets and Systems, 21*, 20–27.

Salama, A. A., ElGhawalby, H., & Ali, S. F. (2017). Topological manifold space via neutrosophic crisp set theory. *Neutrosophic Sets and Systems, 15*, 18–21.

Singh, S., & Wadhwani, S. (2015a). Medical, image denoising using sub band adaptive thresholding techniques based on wavelet 2D transform. *International Journal of Bio-Science and Bio-Technology, 7*(5), 327–334.

Singh, S., & Wadhwani, S. (2015b). Genetic algorithm based medical image denoising through sub band adaptive thresholding. *International Journal of Science, Engineering and Technology Research, 4*(5), 1481–1485.

Smarandache, F. (2016). Degrees of membership >1 and <0 of the elements with respect to a neutrosophic offset. *Neutrosophic Sets and Systems, 12*, 3–8.

Soni, A., & Roy, V. (2014). De-noising of Gaussian noise using discrete wavelet transform. *International Journal of Engineering Trends and Technology, 8*(6), 309–312.

Wang, X.-Y., Yang, H.-Y., Zhang, Y., & Fu, Z.-K. (2013). Image denoising using SVM classification in nonsubsampled contourlet transform domain. *Information Sciences, 246*, 155–176.

Yang, H.-Y., Wang, X.-Y., Niu, P.-P., & Liu, Y.-C. (2014). Image denoising using nonsubsampled shearlet transform and twin support vector machines. *Neural Networks, 57*, 152–165.

Yuan, J. (2018). An improved variational model for denoising magnetic resonance images. *Computers & Mathematics with Applications*, 1–11.

Zhao, R., Luo, Q., & Zhou, Y. (2017). Elite opposition-based social spider optimization algorithm for global function optimization. *Algorithms, 10*(9), 1–21.

Please cite this article in press as: Aravindan, T. E., et al. Medical image denoising by using discrete wavelet transform: Neutrosophic theory new direction. *Cognitive Systems Research* (2018), https://doi.org/10.1016/j.cogsys.2018.10.027